ACS OMEGA

Open Access

http://pubs.acs.org/journal/acsodf

Article

Experimental Study on Rapid Hemostasis Using Peptide Hydrogels

Linru Zeng,* Gan Luo,* Zhenshuang Yue, Yanghua Tang, Zhetian Wang, and Yitie Chang

Cite This: *ACS Omega* 2024, 9, 9247−9255

Read Online

ACCESS | Metrics & More | Article Recommendations

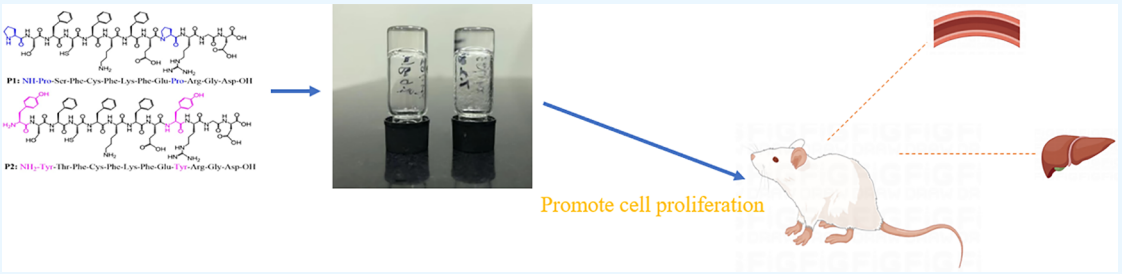

ABSTRACT: Uncontrolled hemorrhaging resulting from trauma, surgery, and disease-associated or drug-induced blood disorders can cause significant morbidities and mortalities in civilian and military populations. Self-assembling peptide nanofibers are particularly attractive due to their rapid and efficient hemostasis, biocompatibility, and wound-healing properties. In this study, we designed two types of 12-residue peptides by using a strong fishnet-like peptide sequence and a pro-cell adhesion sequence (Arg-Gly-Asp, RGD). The peptides are HN2-X-Ser-Phe-Cys-Phe-Lys-Phe-Glu-X-Arg-Gly-Asp-OH (where X is Pro or Tyr), which dissolve in deionized (DI) water and form stable and transparent functional hydrogels. Transmission electron microscopy and scanning electron microscopy demonstrated that the two peptides self-assemble into nanowebs and nanofibers, forming a fishnet-like and three-dimensional network structure. Circular dichroism and Fourier transform infrared spectroscopy analysis demonstrated that the self-assembled peptides mainly adopt a β-sheet structure with β-turn and α-helix as auxiliary assembly growth. 3-(4,5-Dimethylthiazol-2-yl)-2,5-diphenyltetrazolium bromide assay and SEM analysis showed that the cell survival rates were very good, delivering an obvious promotion of cell proliferation of fibroblasts and hepatocytes. Importantly, in vivo hemostasis delivered that the self-assembled peptide nanowebs and nanofibers had a good hemostatic effect on rat saphenous vein and liver bleeding, achieving 38 s faster hemostasis, which was better than commercial "Instantaneous" hemostatic powder. Accoupling the fast hemostasis and effective promotion of liver defect rapid repair, the peptide self-assembly strategy offers a clinically promising treatment option for life-threatening liver bleeding and serves as a renewed impetus for the development of peptide hydrogels as effective hemostatic agents.

1. INTRODUCTION

The design and production of a topical hemostatic agent should be convenient and adaptable to various surgical and postoperative situations, exhibiting rapid efficacy, complete biocompatibility, resorbability, ease of use, and cost-effectiveness.[1−4] Researchers have been exploring the use of natural structural motifs to create nanobiomaterials for hemostasis and tissue engineering. One promising new class of peptide self-assembling topical hemostats, including RADA16, appears to meet all of the desired criteria. Products such as PuraStat and PuraBond, which contain 2.5% RADA16 formulations, have obtained CE certification as Class III medical devices for hemostatic use in humans.[5−11] Recently, PuraSinus, a novel 2.5% aqueous RADA16 formulation, received clearance from the FDA in 2019 as an intraoperative wound dressing designed to promote hemostasis, prevent adhesion formation, and enhance wound healing following nasal surgery or trauma repair (US Food and Drug Administration, 2021).[2,12] However, the nanofibers in this study exhibited unique features of long lengths and straight alignment, allowing them to stack together to form a porous network without the formation of visible nanowebs.[13,14] Therefore, it remains a challenge to develop peptide-based hemostatic materials with precisely controlled mechanical properties that can rapidly and effectively arrest severe ongoing bleeding.

Peptide N-Pro-Ser-Phe-Cys-Phe-Lys-Phe-Glu-Pro-C has been recently reported by Zhao et al. and others.[13,15] The peptide contains only half-sequence ionic self-complementarity, along with turn-making residues of Pro at its termini, to generate turns or bended structures. This results in self-complementary cohesive or staggering ends that facilitate the knitting and tethering of peptide components. The two

Received: October 22, 2023
Revised: January 20, 2024
Accepted: January 25, 2024
Published: February 14, 2024

structurally distinguishable elements consist of two oppositely charged residues, Glu and Lys, which generate electrostatic attraction in an antiparallel strand orientation. The second element contains the key residues Phe-Cys-Phe, serving as the hydrophobic module. At high concentrations, the half-chain complementary peptide can form typical 3D mats or scaffolds with fully packed peptide components. Upon sonication disruption, these 3D mats can be broken down into a "naked mainframe" resembling a nanoscale knitted fabric (nanowebs). Notably, this knitted fabric can be rapidly populated by broken fragments or small-molecule aggregates, reforming the 3D mats through an intermediate interwoven fabric. Due to this property, the peptide-formed hydrogel exhibits self-healing capabilities, enabling it to rapidly stop hemorrhage within minutes. More importantly, the presence of Pro residues at the N and C termini is significant, as Pro lacks N−H moieties available for hydrogen bonding due to its ring structure. This feature often acts as a β-sheet breaker, facilitating the formation of helical structures instead.[12,13] Therefore, the proline residue can effectively hinder β-sheet expansion and prevent the formation of extra fibrils by disrupting the extension of the hydrogen bonding network. Additionally, it bends the peptide chain by forming turns, promoting interfiber staggering and tethering, which are essential for the stabilization of peptide structures.

Furthermore, the Arg-Gly-Asp (RGD) peptide was extensively modified to enhance the speed of hemostasis and wound recovery. This peptide targets integrin receptors on the cell membrane, promoting cell migration and expediting the formation of granulation tissue.[16−21] In a rat liver injury model, the application of 1% RADA16 coupled with the RGD sequence led to more extensive wound healing after 2 weeks compared to thermocautery control sites.[2,22,23] Therefore, it is highly desirable to incorporate the functional moieties RGD within the hydrogel scaffold to maximize the healing efficacy of wound blooding materials. Located at the tenth type III repeating domain of fibronectin, RGD serves as a crucial peptide ligand for the integrin receptor, enhancing cell adhesion and promoting wound healing.[24] It has been established that RGD is a significant motif involved in cell adhesion by interacting with various integrins.[17,25,26] Therefore, hemostatic materials that have been functionalized with RGD exhibit significant potential for specifically sealing blood flow at the site of internal injuries on demand.[27,28]

A series of peptide self-assembling hydrogels was reported recently. The substance can not only have strong biocompatibility but also improve body damage by intervening in a variety of ways and has a high application prospect in various diseases.[29−32] Herein, we design two types of 12-residue peptides (HN-X-Ser-Phe-Cys-Phe-Lys-Phe-Glu-X-Arg-Gly-Asp-OH, where X is Pro or Tyr, P1 and P2 are shown in Figure 1) that P1 peptide contains only half-sequence ionic self-complementarity, along with Pro residues that promote turns and the cell adhesion sequence RGD. Notably, the Pro residues at the N and C termini of P1 lack N−H moieties available for hydrogen bonding due to their ring structure, often serving as β-sheet breakers. In this study, we conducted a series of experiments to verify the hemostatic effect of peptide hydrogels.

2. MATERIALS AND METHODS

2.1. Materials. The peptides were designed and synthesized by Wuhan Haode Biotechnology Co., Ltd. using standard

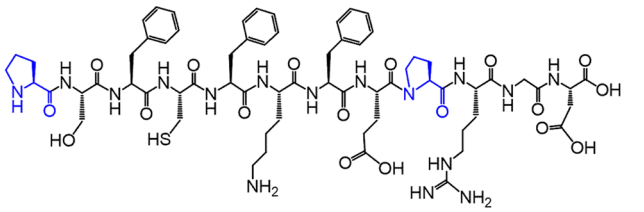

P1: NH-Pro-Ser-Phe-Cys-Phe-Lys-Phe-Glu-Pro-Arg-Gly-Asp-OH

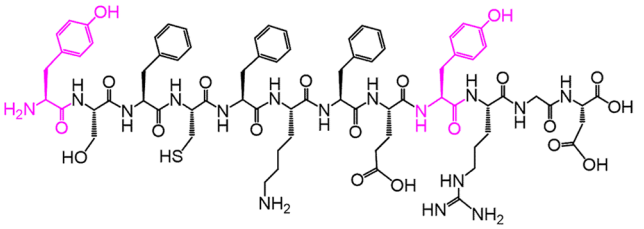

P2: NH_2-Tyr-Thr-Phe-Cys-Phe-Lys-Phe-Glu-Tyr-Arg-Gly-Asp-OH

Figure 1. Chemical structures of two designed peptides (HN-X-Ser-Phe-Cys-Phe-Lys-Phe-Glu-X-Arg-Gly-Asp-OH, where X is Pro or Tyr, P1 and P2).

Fmoc Solid-Phase Chemistry. The peptides were then purified using high-performance liquid chromatography (HPLC) and analyzed using capillary electrophoresis-electrospray mass spectrometry (CE-ESI-MS).[29,31] The amino acid sequences of the peptides are HN-Pro-Ser-Phe-Cys-Phe-Lys-Phe-Glu-Pro-Arg-Gly-Asp-OH (molecular weight 1429.9 Da, purity 95.93%, named as P1) and HN-Tyr-Ser-Phe-Cys-Phe-Lys-Phe-Glu-Tyr-Arg-Gly-Asp-OH (molecular weight 1561.7 Da, purity 95.35%, named as P2). The peptide hydrogels were prepared at a concentration of 10−15 mg/mL (1−1.5 wt %/vol) in DI water (18.2 M, Milli-Q; Millipore) by adjusting the pH to 7.5. The hydrogels were stored at 4 °C until further use. All other chemical reagents used in this study were analytical grade.

The fibroblast cells (L929) and hepatocytes were procured from Hunan Fenghui Biotechnology Co., Ltd. and were cultured in Dulbecco's modified Eagle's medium (DMEM) that was supplemented with 10% fetal bovine serum (FBS) and 1% penicillin/streptomycin. These cells were incubated in a humidified chamber with 5% CO_2 and maintained at 37 °C. The culture media was replaced every other day. The DMEM, live−dead assay kit, and live cell labeling kit were purchased from Thermo Fisher Scientific. Additionally, the Cell Counting Kit-8 (CCK-8) was acquired from Dojindo Laboratories (Japan).

2.2. Transmission Electron Microscopy. The peptide hydrogels were diluted 20-fold and applied directly onto Quantifoil R1.2/1.3 holey carbon mesh on copper grids. Images of the dried grids were captured by using a transmission electron microscope (TEM, JEM-2010, Japan).

2.3. Scanning Electron Microscopy. The peptide hydrogels were diluted 10-fold and then freeze-dried. To enhance the surface conductivity, they were sputter coated with a gold conductive layer. The specimens were imaged by using scanning electron microscopy (SEM, Czech, TENSCAN, MIRA3). Prior to scanning, all specimens were coated with a conductive layer of sputtered gold to enhance the surface conductivity. The operating voltage and current used were 20 kV and 10 mA, respectively.

2.4. Circular Dichroism. The following samples were analyzed using circular dichroism (CD) analysis on a CD spectrometer (Chirascan, Applied Photophysics) equipped

https://doi.org/10.1021/acsomega.3c08310
ACS Omega 2024, 9, 9247−9255

with a 0.1 cm path length quartz cuvette: DI water, 0.20 mg of P1 hydrogel, and 0.15 mg of P2 hydrogel in 350 μL of DI water with pH at 7.5. Initial spectra were recorded at between 190 and 360 nm.

2.5. Fourier Transform Infrared Spectroscopy. The secondary structures of the peptide hydrogels were characterized by using a Fourier transform infrared (FT-IR) spectrophotometer (Nicolet-iS50, Thermo Scientific). The freeze-dried peptides were mounted onto a "Golden Gate" diamond window and their spectra were acquired in the spectral region of 800−3500 cm^{-1}.

2.6. Cell Proliferation and Adhesiveness. The cell proliferations of the P1 or P2 hydrogel were assessed using the CCK-8 (Dojindo Molecular Technologies, Kumamoto, Japan) assay. 50 μL of the P1 or P2 hydrogel was added to 96-well plates. Prior to the cell test, the hydrogels were sterilized using electron beam sterilization radiation followed by immersion in PBS overnight. 100 μL of mouse fibroblast (L929) cell suspension (with a density of 1×10^5 cells/mL) was added to every sample, continuously incubating at 37 °C with 5% CO_2. The culture medium (DMEM with 10% FBS and 1% penicillin/streptomycin) was changed every 2 days. The proliferation rate of L929 cells on hydrogels was tested by a CCK-8 assay following the manufacturer's protocol at scheduled time periods (days 1, 4, and 7).

For the live−dead staining assay (Dojindo Molecular Technologies, Kumamoto, Japan), L929 cells and hepatocytes after days 1, 4, and 7 were stained with Calcein-AM and propidium iodide (PI), respectively, and then observed using a confocal laser scanning microscope. Then, live cells (calcein-AM-stained green) were distinguished from dead cells using PI stained.

SEM observation was continued to exhibit L929 cells culturing on the P1 and P2 hydrogels, with 4 and 7 days fixed with 4% paraformaldehyde and dehydrated with gradient alcohol of 50, 70, 80, 90, 95, and 100%. The dehydrated cells on gels were sprayed gold with a thickness of approximately 5×10^{-6} cm using a Hitachi IB-2 coating unit under a vacuum of 0.1 Torr and examined through SEM observation.

2.7. In Vivo Rapid Hemostasis and Liver Injury Healing. All experimental designs for the animal study were reviewed and approved by the Zhejiang Chinese Medical University Laboratory Animal Research Center (IACUC-20210906-09). The hemostasis experiments in SD rats are divided into two actions. Among them, one is for rapid hemostasis of the great saphenous vein, and the other is for rapid hemostasis and wound healing of the injured liver. For rapid hemostasis of the great saphenous vein, eight male SD rats (200−250 g) were taken and performed with 1% pentobarbital sodium at a dose of 30 mg/kg. Under sterile conditions, bilateral great saphenous veins were exposed from the inguinal approach. After separation of the great saphenous vein, immediately press it with gauze for 3 s and then cover it with hemostatic material. "Instantaneous" hemostatic powder was used as the control group on the left, and P1 or P2 hydrogel was used on the right (4 rats each). No obvious active bleeding at the broken end of the vein was used as the hemostatic standard, and the hemostatic time of each group was recorded, respectively.

Meanwhile, the hemostatic effect of peptide hydrogels on hepatic incision bleeding in rats was investigated. Sixteen male SD rats weighing 200−250 g were taken. Anesthesia was performed with 1% pentobarbital sodium at a dose of 30 mg/kg. Under sterile conditions, the skin, subcutaneous tissue, fascia, and muscle layer were separated layer by layer from the incision under the right costal margin to expose the liver. Resection of the surface of the right liver 5 × 5 mm liver tissue to make a model of liver bleeding. Press the gauze for 3 s and immediately cover it with hemostatic material. In the same way, 8 rats in the control group were treated with "Instantaneous" hemostatic powder, and 4 rats were treated with P1 or P2 peptide hydrogel, respectively. The hemostatic time of each group was recorded with no active bleeding in the liver defect area as the hemostatic standard. After 1 week of hemostasis, SD rats with the above liver bleeding model were killed. The hemostatic properties and injury healing of the liver defect were observed by H&E staining.

2.8. Statistical Analysis. The statistical analysis was conducted using IBM SPSS Statistics 20.0 (SPSS, Chicago, IL) and Origin 8.0 (Origin Lab) software. The results are expressed as the mean ± the standard deviation. Multiple comparisons were performed by using a one-way analysis of variance (ANOVA). The *P*-value less than 0.05 was considered statistically significant.

3. RESULTS AND DISCUSSION

3.1. Preparation and Characterization of Designed Peptide Hydrogels. In this work, we design two types of 12-residue peptides (HN-X-Ser-Phe-Cys-Phe-Lys-Phe-Glu-X-Arg-Gly-Asp-OH, where X is Pro or Tyr, P1 and P2 are shown in Figure 1) that contain only half-sequence ionic self-complementarity together with turn-making residues of Pro and pro-cell adhesion sequences Arg-Gly-Asp (RGD). RGD peptide, as the recognition site of the interaction between integrin and its ligand, mediates the interactions between cells, extracellular matrix, and cell adhesion. Phe-Lys-Phe-Glu peptide shows a strong tendency of β-sheet structure to self-assemble into nanofibers. Cys strengthens the cross-linking and interaction between peptides and fibers, improves mechanical properties and self-healing ability, and also enhances the interaction with cells and tissues. Meanwhile, Pro residue from P1 does not have N−H moieties available for hydrogen bonding by virtue of its ring structure, often conducive to the turning and connection of peptide self-assembling nanofibers to form a complex network structure.[13,15] In contrast, Tyr from P2 is more inclined to β-sheet structure and is conducive to the formation of linear fiber structure.

We dissolved P1 and P2 into DI water with ultrasound and standing to find the supramolecular hydrogel formation. The weights of P1 and P2 are 14.3 and 10.4 mg, respectively, dissolve in DI water with the aid of ultrasound. It was found that P1 dissolved completely after about 1 min and presented a transparent, viscous solution. After ultrasonication for half a minute, P1 statically completes its self-assembly into transparent hydrogels. Meanwhile, P2 is still difficult to dissolve after several minutes of ultrasound. Because Tyr is more hydrophobic, resulting in the enhancement of the overall hydrophobicity of the peptide, it is difficult to dissolve under neutral conditions. Therefore, NaOH solution is slowly added to P2 suspension until the peptide is completely dissolved at pH about 9. Then, dilute HCl solution is added dropwise until a small number of flocs appear, and the ultrasonic dispersion is uniform at pH of about 7.5. After incubation for complete self-assembly, P1 and P2 formed stable and transparent hydrogels in several minutes, as shown in Figure 2.

https://doi.org/10.1021/acsomega.3c08310
ACS Omega 2024, 9, 9247−9255

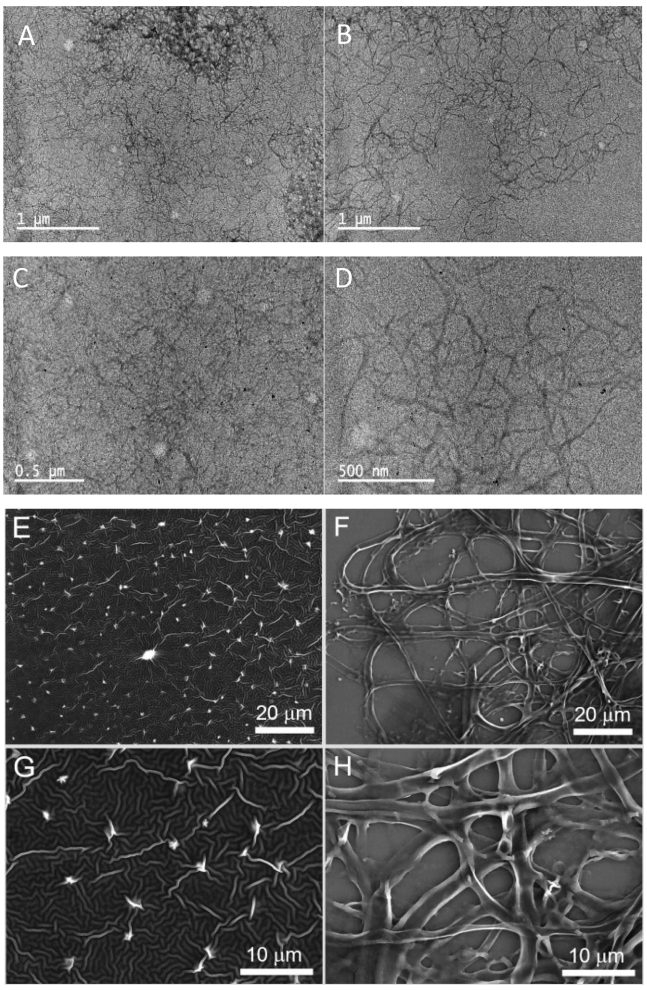

Figure 2. Peptide self-assembling hydrogels, nanowebs, and nanofibers. (A–D) TEM analysis of P1 and P2 self-assembling hydrogels, nanowebs, and nanofibers; (E–H) SEM analysis of P1 and P2 self-assembling nanowebs and nanofibers.

Macroscopic research showed that the peptide hydrogel had good stability and self-healing. Under strong external force, the hydrogels were damaged and became gelatinous. However, it can self-heal and form complete hydrogels in 5 min. The complete microstructures of P1 and P2 by diluted 20 times are shown in Figure 1. The TEM image (Figure 2A–D) showed that P1 and P2 presented different nanowebs or nanofibers. Figure 2A,C shows the microstructure of P1 nanomaterials, as a fishnet-like structure of nanowebs. The nanofiber size and pore size of the nanoweb are homogeneous, with the diameter of nanofiber about 20–40 nm and the pore size of the fishing net about 100–300 nm. Meanwhile, Figure 2B,D shows the microstructure of P2 nanomaterials, as a dense network structure of nanofibers. The nanofibers are uniform with a diameter of about 20–30 nm, and the network structures are complex and dense. Thus, the microstructures of P1 nanowebs and P2 nanofibers are far smaller than the size of cells. The microstructures show it is beneficial to blocking cells and playing a hemostatic role. The SEM image (Figure 2E–H) also presented the microstructures of P1 and P2 self-assembling hydrogels. As shown in Figure 2E,G, the P1 hydrogel showed regular and dense nanofiber and nanoweb structures. The nanofiber diameter was about 500 nm with the pore size of the fishing net about 100–300 nm. The P2 hydrogel showed a fiber network structure with a uniform nanofiber size of 1 μm from Figure 2F,H. The bigger difference in the size from SEM and TEM is the characterization, attributed to the big size of gold particles, leading to the diameter of fiber being especially larger.

Furthermore, we used CD and FT-IR analysis to characterize the secondary structure of the peptides, as shown in Figure 2. The P1 and P2 hydrogels were diluted 200 times and dispersed to detect UV absorption from 190 to 360 nm for investigation. For P1 solution, the negative characteristic wide absorption band at 215 nm and the positive absorption band at 192 nm correspond to the β-sheet secondary structure in P1 nanofibers. The negative absorption band at 202 nm corresponds to the β-turn structure in P1 nanofibers (Figure 3A). The β-turn structure may be mainly a result of the Pro residue for turning and connection of peptide self-assembling nanofibers into complex nanoweb structures.[14,15] On the other hand, the P2 solution showed the negative characteristic wide absorption band at 217 nm and positive absorption band at 194 nm, corresponding to β-sheet formation in P2 nanofibers. P2 nanofibers also show a weak α-helix secondary structure attributed to the negative absorption band at 207 nm (Figure 3B). As shown in Figure 3C, the secondary structures in P1 and P2 hydrogels were detected by FT-IR spectroscopy. P1 and P2 hydrogels showed strong absorption in the β-sheet secondary structure, complying with the characteristic absorption of 1626 (amide I) and 1530 cm^{-1} (amide II) in the FT-IR characteristic absorption spectrum. Meanwhile, the P1 hydrogel shows a wide absorption peak at 1660–1698 cm^{-1} (amide I), delivering a β-turn secondary structure. The slope peak at 1650–1658 cm^{-1} (amide I) shows that the P2 hydrogel has an α-helical secondary structure. Thus, the FT-IR results are basically consistent with that of CD.

Peptide P1 mainly takes a β-sheet secondary structure, orderly stacking growth of molecules through Electrostatic action, hydrogen bond, and $\pi-\pi$ conjugation to form nanowebs structure. The Pro has great potential of β-turning to the tendency of corner secondary structure, cooperating with peptide molecular assembly to form a fishing net nanofibers network. Therefore, as a replacement for Pro, Tyr in peptide P2 has a weak tendency of α-helix secondary structure without disturbing the linear nanofiber structure. Meanwhile, Due to the existence of Cys and other amino acids, there may be a strong interaction between nanofibers and nanofibers network.

3.2. In Vitro Cytocompatibility of Designed Peptide Hydrogels. To investigate the peptide hydrogels hemostasis, it is necessary to systematically evaluate the in vitro and in vivo biocompatibility to verify whether the material has good cell compatibility in vitro and in vivo.[33–35] Therefore, the cytotoxicity, adhesion, and proliferation activities of peptide hydrogels for fibroblasts are comprehensively evaluated.

P1 and P2 hydrogels were cocultured with L929 fibroblast. After 1, 4, and 7 days, the proliferation of cells was observed by CCK-8 methods, laser scanning confocal microscope (LSCM), and SEM. Figure 4A shows that the CCK-8 test determined that the survival rate of L929 fibroblast on P1 and P2 hydrogels was very good in the cytotoxicity test, more than 100% of the blank. As the proliferation time increased, L929 fibroblast cultured on P1 and P2 hydrogels was obviously faster. On the fourth day, the number of L929 cells on P1 and P2 hydrogels was more than 5 times that of the first day. For the 7 days, the number of L929 fibroblasts on P1 and P2 hydrogels was more

https://doi.org/10.1021/acsomega.3c08310
ACS Omega 2024, 9, 9247–9255

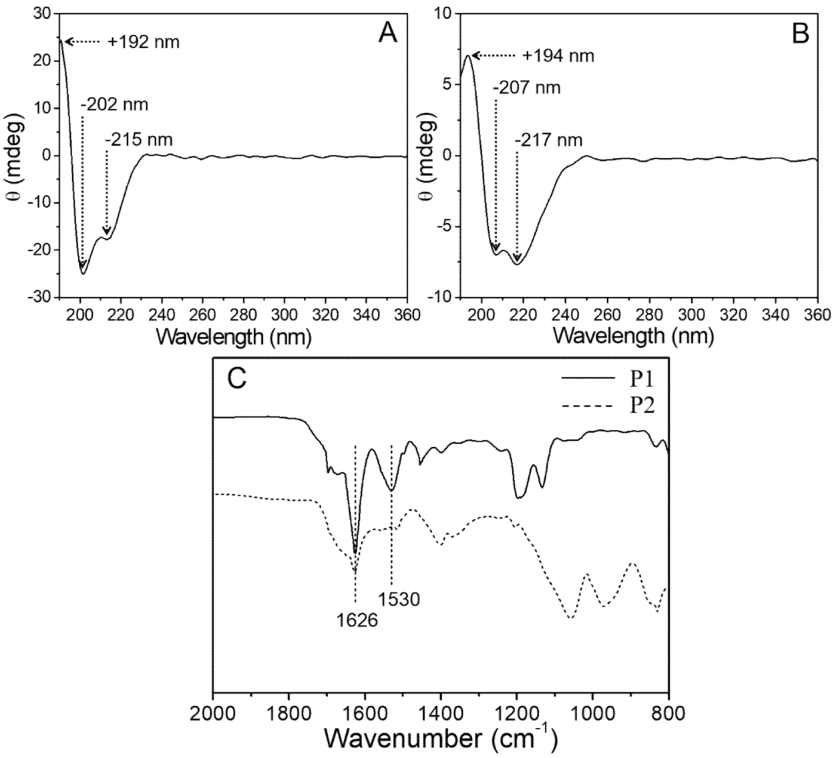

Figure 3. CD spectra and FT-IR spectroscopy of self-assembling P1 and P2. (A) CD spectra of self-assembling P1. (B) CD spectra of self-assembling P2. (C) FT-IR spectroscopy of the self-assembling P1 and P2.

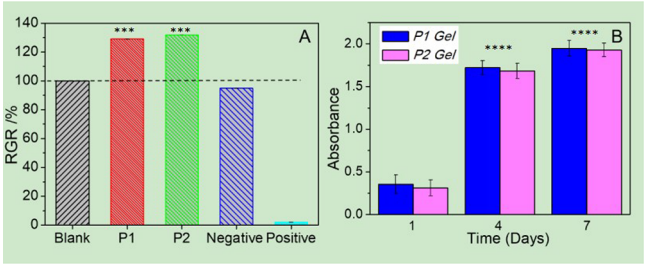

Figure 4. Cytotoxicity and proliferation of L929 cells on P1 and P2 hydrogels and extracts. (A) Cytotoxicity of P1 and P2 hydrogel extracts by the 3-(4,5-dimethylthiazol-2-yl)-2,5-diphenyltetrazolium bromide method. The results showed P1 and P2 hydrogels could significantly promote cell proliferation, but there was no significant difference between them. (B) Proliferation of P1 and P2 hydrogel on days 1, 4, and 7 by CCK-8 assay. The results showed that both P1 and P2 hydrogels could effectively promote cell proliferation with time (p <0.01).

than 6 times that for the first day, determining conducive cell proliferation for P1 and P2 hydrogels (Figure 4B).

Figure 5 shows the results of LSCM. At the first day, the L929 fibroblasts were evenly distributed on P1 and P2 hydrogels. The L929 cells morphology were round or spindle. After the fourth day of proliferation, the L929 cells of P1 and P2 hydrogels migrated and sprouted into a network structure. After that, the network structure P1 or P2 hydrogels and L929 cells filled the culture dishes in 7 days, delivering the cells grew to 100% confluence. With the increase of cell culture time, the morphology of L929 cells on P1 and P2 hydrogels do not change significantly and remain highly proliferation active. Moreover, it is consistent with the above LSCM results from the SEM results (Figure 6). After 4 days of cultivation, the L929 cells on the P1 and P2 hydrogels migrated into network-like structures or cell aggregation packages. After 7 days of coculture, the L929 cells on the P1 hydrogel were basically fulfilled, and the P2 hydrogel was easy to reach saturation. These data show that the L929 cells grow well when cultured with P1 and P2 hydrogels.

Besides, hepatocytes were cocultured with P1 or P2 hydrogels before the next animal wound healing. Figure 7 shows the cell adhesion and proliferation after 1, 4, and 7 days of coculture by LSCM. The coculture of Hepatocytes and P1 or P2 hydrogel on the first day showed a normal cellular state, with less quantity of Hepatocytes but without dead. showing a good state in the P1 or P2 hydrogels cocultured. After 4 days of coculture, the number of hepatocytes showed an increasing trend in P1 and P2 hydrogels. Meanwhile, after 7 days of coculture, the surface of P1 or P2 hydrogel is covered with the hepatocytes with a little amount of death. So, the P1 and P2 hydrogels are good biocompatibility for rapid hemostasis and wound healing in vivo.

3.3. In Vivo Rapid Hemostasis of Injectable Peptide Hydrogels. Herein, we further investigated the hemostatic effect of peptide hydrogels on bleeding of main veins and liver incision, accoupling with wound healing of liver defect in SD rats.[35,36] It was showed that the rapid hemostatic performance from P1 hydrogel, P2 hydrogel, and "Instantaneous" hemostatic powder were very different (Figure 8A). P1 and P2 hydrogels are injectable hydrogels during the animal experimental model in SD rats. Figure 8Ai–iv demonstrated the hemostatic effect of great saphenous vein blooding in SD rats. The hemostatic time of P1 and P2 hydrogels were significantly shorter than that of "instantaneous" hemostatic powder. The fastest hemostatic time of P1 hydrogel was 26 s, the longest was 49 s, and the average hemostatic time was about 38 s. The fastest hemostatic time of P2 hydrogel was 28 s, the longest was 61 s, and the average hemostatic time was

https://doi.org/10.1021/acsomega.3c08310
ACS Omega 2024, 9, 9247−9255

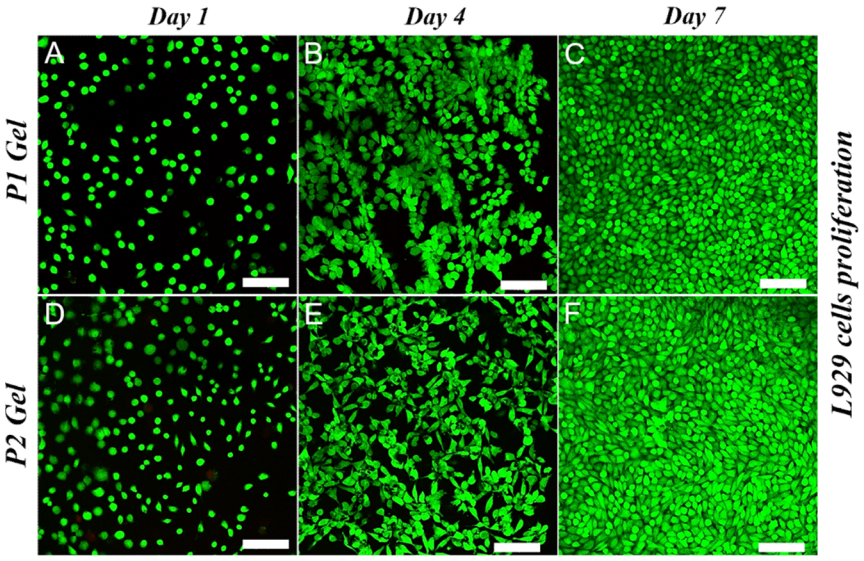

Figure 5. Proliferation of L929 cells on P1 and P2 hydrogels by on Calcein-AM/PI live-stained LSCM. (A) Proliferation of L929 cells on P1 hydrogel on days 1, 4, and 7. The results showed that the cells proliferated massively over time (A−C). (B) Proliferation of L929 cells on P2 hydrogel on days 1, 4, and 7. The results showed that the cells proliferated massively over time (D−F).

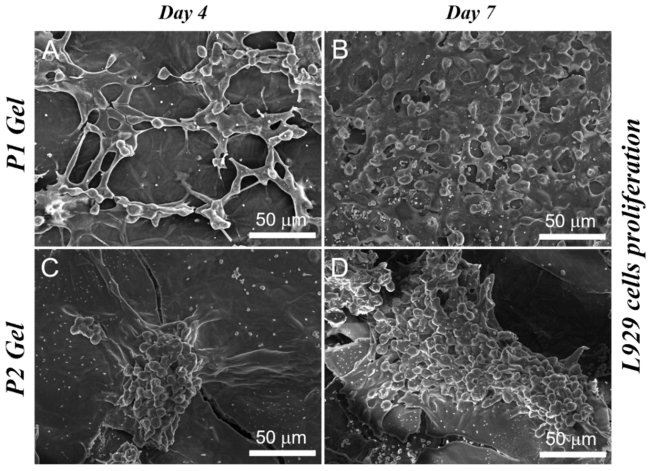

Figure 6. Proliferation of L929 cells on P1 and P2 hydrogels by SEM. (A) Proliferation of L929 cells on P1 hydrogel on days 4 and 7. The results showed that the cells proliferated massively over time (A and B). (B) Proliferation of L929 cells on P2 hydrogel on days 4 and 7. The results showed that the cells proliferated massively over time (C and D).

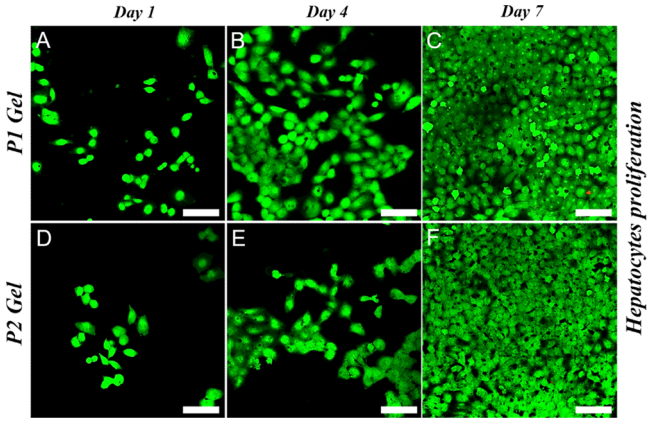

Figure 7. Proliferation of Hepatocytes on P1 and P2 hydrogels by on Calcein-AM/PI live-stained LSCM. (A) Proliferation of hepatocytes on P1 hydrogel on days 1, 4, and 7. The results showed that the cells proliferated massively over time. (B) Proliferation of hepatocytes on P2 hydrogel on days 1, 4, and 7. The results showed that the cells proliferated massively over time.

about 38 s. However, the fastest hemostatic time of "instantaneous" hemostatic powder was 33 s, and the average hemostatic time was 41 s in this study (Figure 8B). Figure 8Av−viii demonstrated their hemostatic effect on liver blooding in SD rats. As shown in Figure 8Av−viii,B, the hemostatic times of P1 and P2 hydrogels and "instantaneous" hemostatic powder are similar for 5 × 5 mm liver bleeding. Both of hemostatic effects are 38.5 s, achieving a 100% hemostatic rate. Thus, the hemostatic effect of injectable peptide hydrogels is better than that of commercialized "instantaneous" hemostatic powder in liver blooding and peripheral blood vessel rupture and bleeding, achieving a rapid and good hemostatic effect.

Based on the characteristics of nanoweb structure, we believe that self-assembling peptide nanomaterials can effectively cover and adhere to bleeding points and surrounding tissues and play a hemostatic role in rapid bleeding caused by most arterial and venous rupture, substantive organ injury, and large-area tissue defect.[37,38] After 1 week of injectable hydrogel implantation, the liver bleeding SD rats were treated with the healing of the liver defect by H&E staining. As shown in Figure 8C, the defective liver area was filled with peptide nanofibers with a large number of fibroblasts, and "hepatocyte-like cells" grew in. Meanwhile, the new tissue in the hydrogel area is grid-like and similar to the normal liver tissue, where a large number of quasi-circular cells similar to hepatocytes can grow. These injectable peptide hydrogels can be well conducive to the repair of liver tissue defects.

4. CONCLUSIONS

In this study, we design two types of 12-residue peptides (HN-X-Ser-Phe-Cys-Phe-Lys-Phe-Glu-X-Arg-Gly-Asp-OH, where X is Pro or Tyr, P1 and P2) that contain only half-sequence ionic

https://doi.org/10.1021/acsomega.3c08310
ACS Omega 2024, 9, 9247−9255

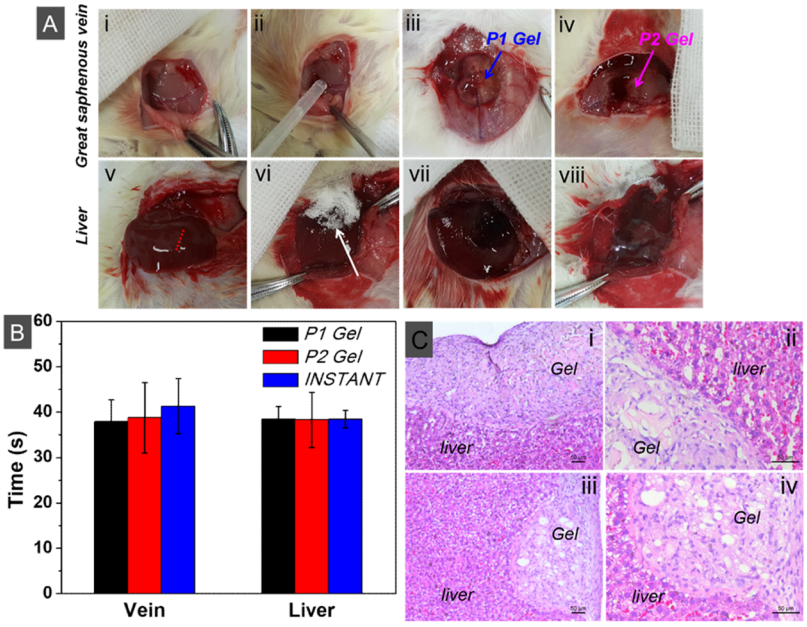

Figure 8. In vivo hemostasis and wound healing of great saphenous vein blooding and liver in SD rats using P1 and P2 hydrogels. (A) In vivo hemostasis of great saphenous vein blooding and liver in SD rats using P1 and P2 hydrogels. (B) In vivo hemostasis time of great saphenous vein blooding and liver in SD rats using P1 and P2 hydrogels. The results showed that P1 and P2 hydrogels showed similar hemostatic effects in the veins, and both were superior to "instantaneous" hemostatic powder. The results showed no significant difference in the hemostatic effect of P1 and P2 hydrogels and "instantaneous" hemostatic powder in the liver. (C) Wound healing of liver in SD rats by using P1 (i, iii) and P2 (ii, iv) hydrogels.

self-complementarity together with turn-making residues of Pro and pro-cell adhesion sequences RGD. Peptide P1 and P2 can self-assemble into nanowebs and nanofibers hydrogels in DI water with pH at 7.5, denoting Pro residue as a β-sheet breaker. Then, P1 and P2 hydrogels show very good biocompatibility to L929 cells and Hepatocytes. Under in vivo hemostasis and wound healing procedures, it demonstrates injectable P1 and P2 hydrogels had good hemostatic effects on SD rat saphenous vein and liver bleeding, better than commercial "instantaneous" hemostatic powder. Meanwhile, injectable peptide hydrogels also showed great efficacy in promoting liver tissue regeneration. Self-assembled peptide hydrogel plays a hemostatic role through the nanoweb or mesh structure barrier, which can be suitable for rapid bleeding caused by most arterial and venous rupture, substantive organ injury, and large-area tissue defects. Peptide hemostatic nanomaterials can have a rapid and effective hemostatic effect, reflecting great advantages and application prospects. In the next step, we will continue to study the hemostatic effect of peptide nanohemostatic materials in other cell and animal models and their intrinsic mechanism of action.

AUTHOR INFORMATION

Corresponding Authors

Linru Zeng − *Department of Orthopedics, Hangzhou Xiaoshan Traditional Chinese Medical Hospital, Hangzhou 311201, P. R. China*; Email: zlr0303@126.com

Gan Luo − *Department of Orthopedics, Hangzhou Xiaoshan Traditional Chinese Medical Hospital, Hangzhou 311201, P. R. China*; orcid.org/0000-0002-2192-5729; Email: luogan0921@163.com

Authors

Zhenshuang Yue − *Department of Orthopedics, Hangzhou Xiaoshan Traditional Chinese Medical Hospital, Hangzhou 311201, P. R. China*

Yanghua Tang − *Department of Orthopedics, Hangzhou Xiaoshan Traditional Chinese Medical Hospital, Hangzhou 311201, P. R. China*

Zhetian Wang − *The Third Clinical Medical College of Zhejiang Chinese Medical University, Hangzhou 310053, P. R. China*

Yitie Chang − *The Third Clinical Medical College of Zhejiang Chinese Medical University, Hangzhou 310053, P. R. China*

Complete contact information is available at: https://pubs.acs.org/10.1021/acsomega.3c08310

Author Contributions

Conceptualization, L.R.Z., G.L., and Y.H.T.; methodology, L.R.Z., G.L., Z.S.Y., Y.H.T., Z.T.W., and Y.T.W.; formal analysis, G.L., Z.S.Y., and Y.H.T.; investigation, L.R.Z., G.L., Z.S.Y., and Y.H.T.; writing−original draft preparation, G.L., Z.S.Y., Y.H.T., Z.T.W., and Y.T.W.; writing−review and editing, L.R.Z., G.L., Z.S.Y., and Y.H.T.; supervision, L.R.Z., G.L., and Y.H.T.; project administration, L.R.Z. and G.L. All authors have read and agreed to the published version of the manuscript.

Notes

The authors declare no competing financial interest.

ACKNOWLEDGMENTS

This work was supported by the Zhejiang Provincial Natural Science Foundation (LGF20H060001).

REFERENCES

(1) Dagi, T. F. The Management of Postoperative Bleeding. *Surg. Clin. North Am.* **2005**, *85* (6), 1191−1213.
(2) Sankar, S.; O'neill, K.; Bagot d'arc, M.; Rebeca, F.; Buffier, M.; Aleksi, E.; Fan, M.; Matsuda, N.; Gil, E. S.; Spirio, L. Clinical Use of the Self-Assembling Peptide RADA16: A Review of Current and Future Trends in Biomedicine. *Front. Bioeng. Biotechnol.* **2021**, *9*, No. 679525.
(3) Kassam, H. A.; Gillis, D. C.; Dandurand, B. R.; Karver, M. R.; Tsihlis, N. D.; Stupp, S. I.; Kibbe, M. R. Development of Fractalkine-Targeted Nanofibers that Localize to Sites of Arterial Injury. *Nanomaterials* **2020**, *10* (3), 420.
(4) Wang, L.; Gong, C.; Yuan, X.; Wei, G. Controlling the Self-Assembly of Biomolecules into Functional Nanomaterials through Internal Interactions and External Stimulations: A Review. *Nanomaterials* **2019**, *9* (2), 285.
(5) 3-D Matrix Europe SAS (2014). PuraStat R Absorbable Haemostatic Material Instructions for Use. Available online at: https://www.nicolai-medizintechnik.de/anweisungen/544_IFU_PuraStat_03_2014.pdf.
(6) Wang, R.; Wang, Z.; Guo, Y.; Li, H.; Chen, Z. Design of a RADA16-based self-assembling peptide nanofiber scaffold for biomedical applications. *J. Biomater. Sci. Polym. Ed.* **2019**, *30* (9), 713−736.
(7) Lee, S.; Trinh, T. H. T.; Yoo, M.; Shin, J.; Lee, H.; Kim, J.; Hwang, E.; Lim, Y.-B.; Ryou, C. Self-Assembling Peptides and Their Application in the Treatment of Diseases. *Int. J. Mol. Sci.* **2019**, *20* (23), 5850.
(8) Gelain, F.; Luo, Z.; Zhang, S. Self-Assembling Peptide EAK16 and RADA16 Nanofiber Scaffold Hydrogel. *Chem. Rev.* **2020**, *120* (24), 13434−13460.
(9) Yi, S.; Ding, F.; Gong, L.; Gu, X. Extracellular Matrix Scaffolds for Tissue Engineering and Regenerative Medicine. *Curr. Stem Cell Res.* **2017**, *12* (3), 233−246.
(10) Yokoi, H.; Kinoshita, T.; Zhang, S. Dynamic reassembly of peptide RADA16 nanofiber scaffold. *Proc. Natl. Acad. Sci. U.S.A.* **2005**, *102* (24), 8414−8419.
(11) Zhao, X.; Nagai, Y.; Reeves, P. J.; Kiley, P.; Khorana, H. G.; Zhang, S. Designer short peptide surfactants stabilize G protein-coupled receptor bovine rhodopsin. *Proc. Natl. Acad. Sci. U.S.A.* **2006**, *103* (47), 17707−17712.
(12) US Food and Drug Administration (2021). 510(k) Premarket Notification K183015, Summary. *Polymer, Ear, Nose and Throat, Synthetic, Absorbable*; PuraSinus R; 3-D Matrix Inc. Available online at: https://www.accessdata.fda.gov/scripts/cdrh/cfdocs/cfpmn/pmn.cfm?ID=K183015 (accessed April 22, 2021).
(13) Ruan, L.; Zhang, H.; Luo, H.; Liu, J.; Tang, F.; Shi, Y. K.; Zhao, X. Designed amphiphilic peptide forms stable nanoweb, slowly releases encapsulated hydrophobic drug, and accelerates animal hemostasis. *Proc. Natl. Acad. Sci. U.S.A.* **2009**, *106* (13), 5105−5110.
(14) Sneer, R.; Weygand, M. J.; Kjaer, K.; Tirrell, D. A.; Rapaport, H. Parallelβ-Sheet Assemblies at Interfaces. *ChemPhysChem.* **2004**, *5* (5), 747−750.
(15) Ruan, L. P.; Luo, H. L.; Zhang, H. Y.; Zhao, X. Investigation on structure and properties of a novel designed peptide. *Macromol. Res.* **2009**, *17* (8), 597−602.
(16) Zhai, Z.; Xu, K.; Mei, L.; Wu, C.; Liu, J.; Liu, Z.; Wan, L.; Zhong, W. Co-assembled supramolecular hydrogels of cell adhesive peptide and alginate for rapid hemostasis and efficacious wound healing. *Nanoscale* **2013**, *5* (7), 2734−2744.
(17) Cheng, T. Y.; Wu, H. C.; Huang, M. Y.; Chang, W. H.; Lee, C. H.; Wang, T. W. Self-assembling functionalized nanopeptides for immediate hemostasis and accelerative liver tissue regeneration. *Soft Matter* **2019**, *15* (42), 8603−8610.
(18) Clevenger, T. N.; Luna, G.; Boctor, D.; Fisher, S. K.; Clegg, D. O. Cell-mediated remodeling of biomimetic encapsulating hydrogels triggered by adipogenic differentiation of adipose stem cells. *J. Tissue. Eng.* **2016**, *7*, No. 2041731416670482.
(19) Clevenger, T. N.; Hinman, C. R.; Ashley rubin, R. K.; Smither, K.; Burke, D. J.; Hawker, C. J.; Messina, D.; Van epps, D.; Clegg, D. O. Vitronectin-Based, Biomimetic Encapsulating Hydrogel Scaffolds Support Adipogenesis of Adipose Stem Cells. *Tissue Eng., Part A* **2016**, *22* (7−8), 597.
(20) Hickman, D. A.; Pawlowski, C. L.; Sekhon, U. D. S.; Marks, J.; Gupta, A. S. Biomaterials and Advanced Technologies for Hemostatic Management of Bleeding. *Adv. Mater.* **2018**, *30* (4), No. 700859.
(21) Humphries, J. D.; Byron, A.; Humphries, M. J. Integrin ligands at a glance. *J. Cell Sci.* **2006**, *119* (19), 3901−3903.
(22) Cheng, T. Y.; Wu, H. C.; Huang, M. Y.; Chang, W. H.; Lee, C. H.; Wang, T. W. Self-assembling functionalized nanopeptides for immediate hemostasis and accelerative liver tissue regeneration. *Nanoscale* **2013**, *5* (7), 2734−2744.
(23) Cheng, T. Y.; Chen, M. H.; Chang, W. H.; Huang, M. Y.; Wang, T. W. Neural stem cells encapsulated in a functionalized self-assembling peptide hydrogel for brain tissue engineering. *Biomaterials* **2013**, *34* (8), 2005−2016.
(24) Sage, E. H.; Bornstein, P. Extracellular proteins that modulate cell-matrix interactions. SPARC, tenascin, and thrombospondin. *J. Biol. Chem.* **1991**, *266* (23), 14831−14834.
(25) Pierschbacher, M. D.; Ruoslahti, E. Cell attachment activity of fibronectin can be duplicated by small synthetic fragments of the molecule. *Nature* **1984**, *309* (5963), 30−33.
(26) PubMed Chada, D.; Mather, T.; Nollert, M. U. The synergy site of fibronectin is required for strong interaction with the platelet integrin alphaIIbbeta3. *Ann. Biomed. Eng.* **2006**, *34* (10), 1542−1552.
(27) Ghosh, S.; Tripathi, A.; Gayen, P.; Sinha roy, R. Peptide-based topical agents and intravenous hemostat for rapid hemostasis. *RSC Med. Chem.* **2020**, *11* (10), 1100−1111.
(28) Lee, D. H.; Blajchman, M. A. Novel platelet products and substitutes. *Transfus. Med. Rev.* **1998**, *12* (3), 175−187.
(29) Chen, C. S.; Xu, X. D.; Wang, Y.; Yang, J.; Jia, H. Z.; Cheng, H.; Chu, C. C.; Zhuo, R. X.; Zhang, X. Z. A Peptide Nanofibrous Indicator for Eye-Detectable Cancer Cell Identification. *Small* **2013**, *9* (6), 920−926.
(30) Chu, B.; He, J. M.; Wang, Z.; Liu, L. L.; Li, X. L.; Wu, C. X.; Chen, C. S.; Tu, M. Proangiogenic peptide nanofiber hydrogel/3D printed scaffold for dermal regeneration. *Chem. Eng. J.* **2021**, *424*, No. 128146.
(31) Chen, C. S.; Zeng, F.; Xiao, X.; Wang, Z.; Li, X. L.; Tan, R. W.; Liu, W. Q.; Zhang, Y. S.; She, Z. D.; Li, S. J. Three-Dimensionally Printed Silk-Sericin-Based Hydrogel Scaffold: A Promising Visualized Dressing Material for Real-Time Monitoring of Wounds. *ACS Appl. Mater. Interfaces.* **2018**, *10* (40), 33879−33890.
(32) Chen, C. S.; Xu, X. D.; Li, S. Y.; Zhuo, R. X.; Zhang, X. Z. Photo-switched self-assembly of a gemini α-helical peptide into supramolecular architectures. *Nanoscale* **2013**, *5* (14), 6270−6274.
(33) Hao, R.; Peng, X.; Zhang, Y.; Chen, J.; Wang, T.; Wang, W.; Zhao, Y.; Fan, X.; Chen, C.; Xu, H. Rapid Hemostasis Resulting from the Synergism of Self-Assembling Short Peptide and O-Carboxymethyl Chitosan. *ACS Appl. Mater. Interfaces.* **2020**, *12* (50), 55574−55583.
(34) Wei, S.; Chen, F.; Geng, Z.; Cui, R.; Zhao, Y.; Liu, C. Self-assembling RATEA16 peptide nanofiber designed for rapid hemostasis. *J. Mater. Chem. B* **2020**, *8* (9), 1897−1905.
(35) Carter, T.; Qi, G.; Wang, W.; Nguyen, A.; Cheng, N.; Ju, Y. M.; Lee, S. J.; Yoo, J. J.; Atala, A.; Sun, X. S. Self-Assembling Peptide Solution Accelerates Hemostasis. *Adv. Wound Care* **2021**, *10* (4), 191−203.
(36) Yan, J.; Wang, Y.; Li, X.; Guo, D.; Zhou, Z.; Bai, G.; Li, J.; Huang, N.; Diao, J.; Li, Y.; et al. A Bionic Nano-Band-Aid Constructed by the Three-Stage Self-Assembly of Peptides for Rapid Liver Hemostasis. *Nano Lett.* **2021**, *21* (17), 7166−7174.
(37) Zhu, J.; Han, H.; Li, F.; Wang, X.; Yu, J.; Qin, X.; Wu, D. Peptide-Functionalized Amino Acid-Derived Pseudoprotein-Based Hydrogel with Hemorrhage Control and Antibacterial Activity for Wound Healing. *Chem. Mater.* **2019**, *31* (12), 4436−4450.

https://doi.org/10.1021/acsomega.3c08310
ACS Omega 2024, 9, 9247−9255

(38) Hainline, K. M.; Fries, C. N.; Collier, J. H. Progress Toward the Clinical Translation of Bioinspired Peptide and Protein Assemblies. *Adv. Healthcare Mater.* **2018**, 7 (5), No. 700930.

https://doi.org/10.1021/acsomega.3c08310
ACS Omega 2024, 9, 9247−9255